Computer aided kinematic analysis of fault sets

Computerunterstützte kinematische Störungsanalyse

H. PERESSON

with 5 Figures and 3 Tables

Keywords:

Computer software
Brittle tectonics
Fault kinematics
Reichraming nappe

Schlüsselwörter:

Computerprogramme
Sprödtektonik
Störungskinematik
Reichraminger Decke

Address of the author:

Mag. Herwig Peresson
Institut für Geologie der Universität Wien
Universitätsstraße 7/III
A-1010 Wien

Mitt. Ges. Geol. Bergbaustud. Österr.	38	S. 107–119	Wien, 1992

Contents

Inhalt

Zusammenfassung

Es werden drei Computerprogramme zur kinematischen Analyse von Harnischflächen vorgestellt. Diese Programme erlauben eine Klassifikation des Bewegungscharakters sowie eine Trennung mehrphasiger Datensätze in Untergruppen mit kogenetischen Störungsflächen. Zur Bestimmung der Einengungs- und Extensionsrichtung einer Untergruppe werden für jede Harnischfläche die inkrementellen Strainachsen (P-, B- und T-Achsen) berechnet. Der Winkel Theta zwischen der Verkürzungs(P)-Achse und der Störungsfläche kann beliebig gewählt werden. Kinematische Strain-Achsen werden mit Theta = 45° berechnet. Für konjugierte Störungen kann eine Bestimmung der dynamischen Stress-Achsen mit jenem Theta-Winkel erfolgen, für den der Regelungsgrad aller P-Achsen am größten ist. Die Achsen werden graphisch in einem Schmidt'sches Netz dargestellt. Ihre Verteilung gibt Aufschluß über den Deformationstyp und die Form der Strainellipse. Die Schwerpunktvektoren der P- und T-Achsenverteilungen ergeben die Einengungs- und Extensionsrichtung eines kogenetischen Datensatzes. Die Methode wird an einem Beispiel aus den Kalkalpen veranschaulicht. Ein Vergleich der Resultate mit komplexeren, dynamischen Paläostressanalysen ergibt eine gute Übereinstimmungen.

Abstract

Three computer programs are presented which allow an accurate analysis of fault-slip data (slickensides). This contains classification of the movement character as well as separation of polyphase data sets into different subsets containing kinematic compatible faults. To determine the shortening and extension direction of one subset the incremental strain axes (P-, B- and T-axes) of each fault are computed. The angle Θ (Theta) between the fault plane and the P-axis can be chosen depending on whether a kinematic or a dynamic analysis is carried out. Incremental strain axes are calculated by using $\Theta = 45°$. A dynamic evaluation of stress axes can be done in case of newly formed conjugate faults. These axes are constructed with the best fit Θ-angle which minimizes the directional scatter of all individual P- or T-axes. The determined axes are plotted into an equal area net. Their orientation provides information about the type of deformation (normal, reverse and strike-slip faulting). Distribution patterns of the axes allow to estimate the shape of the strain ellipse. The center-of-gravity vector of all P- and T-axes vectors is considered to give the most probable shortening- and extension direction of one fault set. The method was tested on a polyphase fault set from the Northern Calcareous Alps. Results are compared with more complex paleostress analyses and show very similar values.

1. Introduction

In brittly deformed rocks, slickensides are the most common and most important source of information to determine the kinematic and/or paleostress history in the area of investigation (HANCOCK 1985). These slickensides contain the movement vector of adjacent blocks. The first attempt to relate fault geometry and kinematics to driving stresses has been done by ANDERSON (1951). More recently, numerous inverse methods have been developed using fault-slip data to reconstruct paleostress fields. This analysis is done either by numerical techniques (e.g. ETCHECOPAR et al. 1981, ARMIJO et al. 1982, ANGELIER 1979, 1984, MICHAEL 1984, RECHES 1987, WALLBRECHER & FRITZ 1989) or graphical techniques (ARTHAUD 1969, ANGELIER & MECHLER 1977, ALEXANDROWSKI 1985, LISLE 1987). Following BOTT (1959), all dynamic inversion methods are based on the fundamental assumption that fault-slip occurs in the direction of the maximum resolved shear stress acting on a fault plane. In consequence fault striation is always considered to represent the direction of maximum shear stress. The inverse methods compute the best fit reduced stress tensor – defined by the directions and relative magnitudes of the three principal stress axes – which minimizes the deviation angles between the observed striations and the theoretical slip directions for a given set of fault planes.

Dynamic versus kinematic analysis

Fundamental assumptions of all dynamic methods are that stress is homogeneous and that faults do not interact mechanically. For a detailed discussion see ETCHECOPAR et al. (1981) or ONCKEN (1988). MARRETT & ALLMENDINGER (1990) pointed out the significance of strain compatibility between two differently oriented faults which requires that slip must occur parallel to their line of intersection if no additional structures are formed. The problem arises in polyphase deformed rocks. Slip on reactivated faults could be rather controlled by strain compatibility than by resolved shear stresses. For example, this has been shown by CASAS-SAINZ & SIMÓN-GÓMEZ (1992).

In contrast to dynamic paleostress analyses a kinematic analysis tries to find out shortening and extension directions in faulted rocks (i.e. strain axes) or transport directions of rock units without any regard to applied stresses. For kinematic analyses the principle incremental strain axes of a given fault can

be used which are commonly referred to as P-, B- and T-axis (Fig. 2). The names P- and T-axis are unfortunate, because they suggest the stress terms 'pressure' and 'tension' used in fault plane solutions by seismologists. Nevertheless, I will use the terms in this paper always referring to shortening and extension axes, which are fundamentally kinematic, although stress and strain axes can coincide in special cases. Coaxiality of stress and finite strain axes exists in pure shear regimes with conjugate faults. This is not the case in simple shear zones where only the incremental strain axes of small displacements are coaxial with stress (WOJTAL & PERSHING 1991). The finite strain axes then are rotated in respect to stress axes.

In this paper three computer programs are presented, which provide facilities for data handling, kinematic fault-slip interpretation and graphical presentation. These are as follows:

Program CORRECT:

* Correction of measurement errors of fault-slip data.
* Calculation of the pitch-angle defined as the angle between the strike-direction of the fault plane and the movement vector.
* Classification of the character of slip on each individual fault using the sense-of-movement and the pitch-angle.

Program FAULT

* Identification of kinematically compatible faults.
* Separation and splitting of heterogeneous fault sets into different subsets from the computer screen.
* Rapid graphical presentation of the data. This includes the output of DXF-files compatible with commercial graphic programs (for example AUTOCAD or CORELDRAW).

Program STRAIN

* Computation of the P- and T-axes for each individual fault.
* Statistical analysis of the P- and T-axes distribution for fault sets.
* Calculation of the center-of-gravity vector of the P- and T-axes giving the main shortening and extension axes for a homogeneous fault set.

Data collection

In a limited outcrop dip directions and dip angles of fault planes and striations are measured. Shear sense indicators such as offset markers, fibrous minerals grown behind fault steps, riedel shears, slickolithes or tension gashes are used to decide the sense-of-movement on a fault plane (PETIT 1987). Overprinting relationships such as different striations or growth of differently oriented fibres on the same fault plane are noted in order to establish a relative chronology of faulting in multiply deformed sequences and to aid separation of inhomogenous fault sets. Additional information concerning deformation history is derived from tension gashes, joints, stylolithes, fold axes and the orientation of bedding planes (e. g. RAMSAY & HUBER, 1983; HANCOCK, 1985). Orientations of these structures are recorded as well as their relative ages in respect to individual fault planes.

2. Correction of measurement errors and classification of fault-slip data

The first step in data processing is the input of measured orientations of fault planes and related slickenlines into the program CORRECT. The shear-sense of the faults can be specified by <S> (sinistral) or <D> (dextral) for the opposite block, by <R> (reverse) or <N> (normal) for the hanging wall block, or by a blank (unknown). The certainty of the sense-of-movement can be weighted by using small or capital letters. Due to measurement errors the striation often does not coincide with the fault plane. Striations are therefore corrected by computing the intersection line of the fault plane with the plane containing the measured striation and the pole to the fault. In the next step the pitch-angle (δ) between the strike direction of the fault plane and the striation is calculated by using the formula:

$$tan\delta = \frac{tan(\alpha_s - \alpha_f - \pi/2)}{cos\beta}$$

where α_s denotes the dip direction of the striation, α_f the dip direction and β the dip angle of the fault plane. The pitch-angle is positive in the upper left and lower right quadrant and negative in the two other quadrants of the fault surface of the footwall block (Fig. 1).

In connection with the sense-of-movement of the hanging wall block a classification of the slip vector is made. Pitch = 0° denotes pure strike-slip, pitch = 90° denotes pure dip-slip movement. The fault plane of the footwall block is subdivided into 12 segments, each containing an interval of 30°. For example, a normal fault with a pitch-angle of -63° will be classified as normal-dextral (ND) with the main

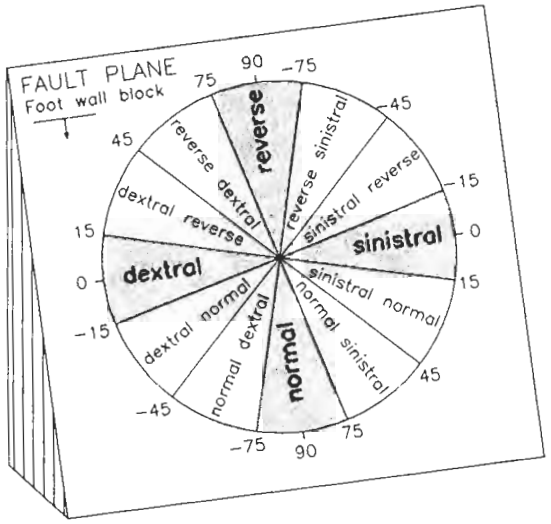

Fig. 1: Classification of the slip direction on fault planes according to the pitch angles and the sense-of-movement used in program CORRECT.

component of movement named first. Table 1 shows a printer output of the program CORRECT.

3. Separation of polyphase fault populations

Dynamic or kinematic analyses are valid only with homogeneous data sets. The complete data set which may contain multiple generations of faults and striations has to be separated into subsets before running any analytical process, either a paleostress or kinematical determination. Although some paleostress programs automatically separate inhomogeneous fault sets the result is often artificial, especially if only a small amount of faults have been collected. A pre-separation procedure taking into account all field observations more likely leads to a satisfying separation of cogenetic faults.

The program FAULT plots the previous classified data in an equal area net on the computer screen. Faults are displayed either as great circles with the related striations or with the pole to the plane and a short segment of the 'movement plane' running through the pole and the striation (HOEPPENER 1955). Four different colours mark the main component of the sense-of-slip (dextral = red, sinistral = green, reverse = blue, normal = pink). Selective data plotting according to the pitch-angles or to the sense-of-movements is optional. It is possible to filter out faults with similar characteristics from the original data set – for example, faults with a pitch angel lower than 20° to figure out strike-slip faults. The advantage is an easy identification of kinematic compatible faults.

Following ANDERSON (1951) three different main types of conjugate fault sets occur depending on the orientation of the three principle stress axes ($\sigma_1 > \sigma_2 > \sigma_3$). Compressional regimes are expressed either by strike-slip faults (shortening and extension axes horizontal) or by reverse and thrust faults (shortening axis horizontal, extension axis vertical). Extensional tectonics generate normal faults (shortening axis vertical, extension axis horizontal). After the identification of different subsets in an inhomogeneous fault set the program FAULT allows a quick separation of individual slickensides. Faults are selected directly from the equal area plot displayed on the computer screen. All data of one subset can be saved to a separate data file for further use.

4. Kinematic and dynamic interpretation

In the final step the P- and T-axes are computed for each individual fault of a subset, using the orientation of fault planes and striations, the pitch angel and the sense of shear. The aim is to evaluate the mean shortening- and extension direction of one subset. The construction of the shortening and extension axes is simple (Fig. 2).

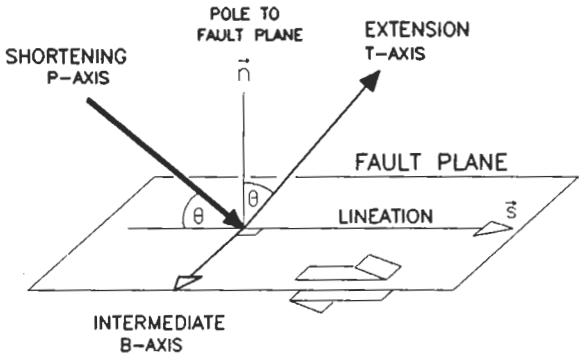

Fig. 2: Orientation of the principle incremental shortening and extension axes in respect to a fault plane. The angle Theta (Θ) is 45°.

Each pair of axes lies in the 'movement plane' which is perpendicular to the fault plane and contains the slip vector (striation). The P-axis makes an angle Θ (Theta) with the fault plane, the T-axis is perpendicular to the P-axis and respectively makes an angle 90°-Θ with the fault plane. The B-axis or intermediate axis is perpendicular to both other axes and always lies within the fault plane, perpendicular to the striation. Neither shortening nor extension occurs in the B-axis direction in the case of plane strain deformation. In fault plane solutions and kinematic analysis a Θ-angle of 45° is used (MARRET & ALLMENDINGER 1990) which gives the principal incremental strain axes of each fault. Here, I assume that the amount of slip on individual slickensides is

Table 1: Output of the program CORRECT. Orientation of all fault planes and slickenlines from the test site (N = 66) – from left to right – column 1: Reference number; column 2: Fault plane (dip direction / dip angle); column 3: measured striation on fault plane; column 4: Corrected striation rotated into fault plane; column 5: computed pitch-angle (angle between strike direction of fault plane and striation); column 6: field determined shear-sense and calculated movement direction according to the pitch-angle (see Fig. 1) – R = reverse, N = normal, D = dextral, S = sinistral sense-of-slip. Oblique slip is marked by a combination of letters with the dominant movement named first (e.g RS = reverse-sinistral). Capital letters denote certain and small letters uncertain determined sense-of-slip.

Nr.	plane	striae	corr. striae	pitch	shear-sense	
1	45/76	10/76	14/74	82	r	r
2	164/65	200/60	199/60	–74	R	RS
3	60/40	40/38	40/38	74	R	RD
4	120/28	40/8	41/6	12	d	d
5	45/45	56/43	57/44	–81	R	R
6	12/52	30/50	30/51	–79	R	R
7	170/66	204/65	200/63	–77	r	r
8	50/60	66/57	66/59	–82	R	R
9	220/65	216/64	215/65	88	R	R
10	40/45	33/44	32/45	84	R	R
11	212/60	212/60	212/60	–90	R	R
12	214/50	214/50	214/50	–90	R	R
13	40/30	41/33	41/40	–89	R	R
14	34/52	34/52	34/52	–90	R	R
15	240/70	226/69	225/69	85	R	R
16	240/72	220/70	220/71	84	R	R
17	205/75	220/72	221/74	–86	R	R
18	61/54	57/53	57/54	88	R	R
19	40/75	40/75	40/75	–90	R	R
20	200/42	208/39	209/42	–83	R	R
21	195/60	196/58	195/60	–90	R	R
22	70/36	149/9	149/8	–14	r	s
23	124/30	130/30	131/30	–84	R	R
24	145/42	155/40	155/42	–83	r	r
25	216/35	134/7	135/6	11	d	d
26	200/37	130/30	138/20	34	r	dr
27	140/40	154/38	154/39	–79	r	r
28	160/66	130/65	132/63	78	R	R
29	195/60	125/24	122/26	31	r	dr
30	145/42	157/43	157/41	–81	r	r
31	15/75	95/32	95/32	–34		
32	160/78	73/15	73/15	14		
33	350/85	264/37	264/37	39		
34	245/60	303/42	303/42	–51	r	rs
35	225/60	272/50	272/50	–62	r	rs
36	188/30	265/5	266/7	–14	R	S
37	255/55	290/50	290/49	–68	r	rs
38	216/35	278/16	279/18	–32	r	sr
39	200/37	110/3	111/1	1	D	D
40	45/45	88/32	90/35	–55	R	RS
41	22/56	97/20	97/20	–26	R	SR
42	350/47	72/7	73/8	–10	S	S
43	340/50	290/42	293/39	55	R	RD
44	355/56	285/25	284/26	32	R	DR
45	12/52	83/18	85/20	–26	R	SR
46	195/60	125/24	122/26	31	r	dr
47	170/66	80/10	84/9	10	r	d
48	245/80	156/15	158/15	17	s	sn
49	160/88	71/13	70/13	13	D	D
50	198/88	106/4	108/4	4	S	S
51	206/80	117/5	117/5	6	S	S
52	340788	252/7	250/7	7	d	d
53	195/66	110/12	110/12	12	s	s
54	350/75	73/17	75/17	–19	D	DN
55	340/70	259/25	260/25	27	D	DR
56	335/80	63/6	64/6	–6	d	d
57	160/85	72/11	71/11	11	D	D
58	355/63	2/63	2/63	–87	N	N
59	350/62	354/62	355/62	–88	N	N
60	352/58	356/60	356/58	–88	N	N
61	225/77	200/70	192/75	82	N	N
62	214/70	160/62	164/60	68	N	NS
63	189/61	162/60	164/59	77	N	N
64	6/68	343/64	341/66	80	n	n
65	144/62	210/39	209/38	–45	n	dn
66	168/64	210/46	218/53	–62	N	ND

of the same magnitude and relative low in respect to the outcrop area. Dominant faults with larger offsets can be statistically expressed with more measurements. Therefore, no weighting factor regarding the amount of slip on individual faults is necessary. A relationship between stress and strain axes can be made under the assumption that slip on fault planes is low and deformation is coaxial. Therefore, the principle axes of the finite state of strain are comparable to those of small strain increments and to paleostress axes.

In order to make a pure dynamic analysis using conjugate faults to reconstruct the stress axes, we can choose an angle which is half the angle between the two sets. Mohr-Coulomb type faults always show angles between σ_1 and the fault less than 45° which depends on the angle of internal friction. Conjugate fault sets often include an angle of about 30°. It should be noted that speaking in terms of stress the application of the simple P-T-axes method is only reliable with newly formed faults. The direction of slip on reactivated fault planes depends on the orientation and the relative magnitudes of the principal stress axes (BOTT 1959) which is not considered in this calculation. Nevertheless the P-T-axes method yields robust results, especially if the data show preferred orientations in two conjugate fault sets, whereas in this case the numerical inverse method often fails. As mentioned above, in case of conjugate faults the stress and finite strain axes can be considered as being coaxial. Another advantage of the P-T-axes method is, that only few data are required to ana-

lyse fault kinematics, whereas stress inversion based on BOTT's formula needs a large amount of fault-slip data to get meaningful results. The program STRAIN calculates the P-, B- and T-axes of each slickenside of one fault population (tab. 2). The Θ-angle can be chosen between 0° and 90° depending on carrying out a kinematic analysis with Θ = 45° or a dynamic analysis using the best fit Θ-angle.

P- and T-axes distribution

The calculated axes for all individual planes of a subset are plotted into an equal area net on the computer screen. They are considered as unit vectors and their directional distributions are statistically analysed using the 'Regelungsgrad' R% (WALLBRECHER 1986) given by:

$$R\% = \frac{2|\vec{R}|-N}{N} * 100$$

$|\vec{R}|$ denotes the vector sum of all unit vectors and N denotes the number of faults. The value of R% lies between 0% and 100% expressing the homogenity of the P-, B- and T-axes distribution. R%=100% denotes complete coaxiality of all individual P-axes (resp. B-, T-axes), R% = 0% expresses an absolute heterogeneous orientation. Changing the Θ-angle will affect the R%-value. The best fitting Θ-angle of a specific data set is found if R% reaches the highest possible value (Fig. 3).

In a dynamic analysis using conjugate faults this Θ-angle can be chosen to calculate the principle stress axes σ_1, σ_2, σ_3. The R%-value allows a rough estimation of the shape of the strain ellipsoid. In case of triaxial strain ($e_1 > e_2 > e_3$) the P-, B-, and T-axes are concentrated in three distinct clusters, whereas uniaxial shortening ($e_1 > e_2 = e_3$) produces a preferred orientation of the shortening (P)-axes in connection with a more heterogeneous T-axes distribution. The T- and B-axes show a more or less great circle distribution.

Determination of the mean shortening- and extension direction

The best fitting mean shortening- and extension direction for the whole data set is considered to be represented by the center-of-gravity vector of all individual P- and T-axes. In the case of triaxial strain the three center-of-gravity vectors of the P-, B- and T-axes distribution should be nearly perpendicular to each other, whereas in the case of uniaxial strain the center-of-gravity vector of the B- and T-axes (resp. B- and P-axes) could be meaningless due to their almost great circle-like distribution. The advantage of this method is that the result is only little affected

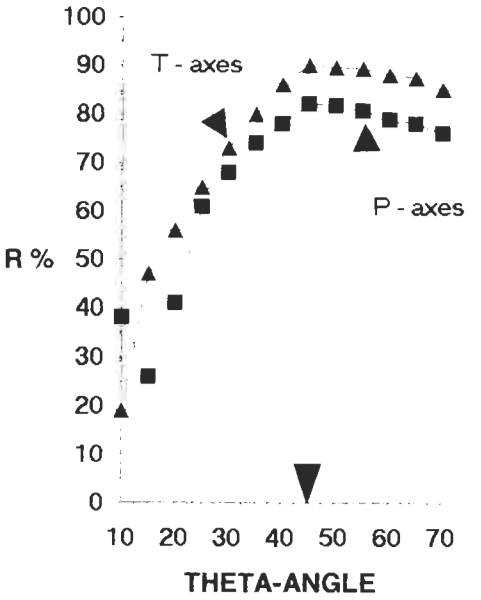

Fig. 3: Plot of R% (diversity factor of P- and T-axes distribution) versus Theta-angle showing a best directional arrangement of P- and T-axes at Theta = 45° for fault set 1 (see Fig. 5).

by single faults which do not fit into the fault population (which P-axis deviates from most others). The center-of-gravity vector is highly independent of the used Θ-angel if the data set consists of conjugate faults with an equivalent developement of both sets. In contrast, it is obvious that the chosen Θ-angel will have large influence on the result if a data set consists of only one parallel set of faults.

The second method used for determination of the average strain axes is density grid counting of each distribution after an algorithmus proposed by ROBIN & JOWETT (1986). In this case, satisfying results can only be expected by using a larger amount of data. The peak position of the density grid gives the most probable orientation of the mean strain axes, but it does not take into account axes which deviate from this position.

5. Field example

The method was tested by a fault set measured in an outcrop of Late Triassic dolomite situated in the Reichraming nappe of the Northern Calcareous Alps (Upper Austria) – Fig. 4. The test site is located near the thrust front of the Weyer Arc which forms a complex anticlockwise rotated part of the Northern Calcareous Alps (DECKER et al., in prep.). Folding and faulting of the well-bedded dolomite occurred during Cretaceous and Tertiary thrusting. 66 slickensides have been measured (Tab. 1).

Overprinting slickenlines point to multiple reac-

Table 2: Output of the program STRAIN (fault set 1). Computed P- (shortening), B-(intermediate) and T-(extension) axes of each fault of subset 1 using Theta = 45° (see Fig. 2). Calculated principle strain axes: e_1 (shortening) = 217/07, e_2 (intermediate) = 126/03, e_3 (extension axis) = 004/84. R = directional distribution factor of P-, B- and T-axes.

nr.	plane	striae	pitch	B-axis	P-axis	T-axis	dev.	mov.
1	45/76	5/72	78.5	132/11	35/30	240/58	36.58	r
2	164/65	199/60	-73.5	81/15	176/18	314/66	41.34	RS
3	60/40	40/38	74.4	138/10	229/6	350/78	12.18	RD
4	120/28	41/6	12.4	134/27	244/33	14/45	36.60	d
5	45/45	57/44	-81.5	321/6	231/1	132/84	15.24	R
6	12/52	30/51	-78.7	289/9	20/7	147/79	21.52	R
7	170/66	200/63	-76.8	85/12	180/20	326/66	38.11	r
8	50/60	66/59	-81.8	324/7	56/15	210/73	28.77	R
9	220/65	218/65	89.2	310/1	220/20	43/70	13.82	R
10	40/45	34/45	85.7	127/3	37/1	289/87	7.54	R
11	212/60	212/60	-90.0	122/0	212/15	32/75	9.67	R
12	214/50	214/50	-90.0	304/0	214/5	34/85	3.15	R
13	40/30	43/30	-87.4	312/1	222/15	46/75	9.90	R
14	34/52	34/52	-90.0	124/0	34/7	214/83	13.82	R
15	240/70	228/70	85.8	329/4	237/25	67/65	26.75	R
16	240/72	220/71	83.6	328/6	235/27	70/62	26.82	R
17	205/75	224/74	-84.9	116/5	209/30	17/59	24.57	R
18	61/54	59/54	88.8	150/1	60/9	246/81	27.89	R
19	40/75	40/75	-90.0	310/0	40/30	220/60	36.67	R
20	200/42	210/42	-82.5	116/5	25/3	264/84	15.13	R
21	195/60	199/60	-88.0	106/2	196/15	9/75	22.06	R

max dev: = 41.3°, min dev: = 3.1°, mean dev: 22.3°
P axis (e_1): 217/07; R = 83 %
B axis (e_2): 126/03; R = 88 %
T axis (e_3): 004/84, R = 90 %

tivations of individual faults and makes it possible to establish a relative chronology of the deformation events. The orientation of fault planes is not related to the orientation of bedding planes which are intensively folded. It can be shown by an easy fold test as proposed by MARRETT & ALLMENDINGER (1990) that faulting postdates folding of the dolomite beds. Kinematically compatible faults have been separated into 5 different subgroups of the original data set. Shortening and extension directions have been obtained by using the P-T-axes method. The results are compared with other methods in figure 5.

From old to young the following deformations are recorded (Fig. 5):

(1) Set 1 consists of conjugate NW-SE striking faults mostly dipping between 40° to 60° towards the NE and SW. Senses-of-movements are reverse. Deformation is of thrust type with a shortening direction NE–SW and a subvertical extension direction.

(2) Set 2 contains faults which dip moderately to SE. They clearly cut all faults of set 1 and are therefore younger. Sense-of-slip is reverse and deformation again is of thrust type with shortening directed NW-SE and extension oriented subvertically.

Due to the position near to the thrust front of the Weyer Arc, which underwent a considerable anticlockwise rotation after the Late Eocene, set 1 and 2 are rotated passively about 45° clockwise due to dragging. This can be derived by comparisons with data outside the dragged zone.

(3) Slickensides of set 3 are characterized by a second oblique striation occuring on reactivated faults of set 1 and on tilted bedding planes. Shortening is directed E–W, extension again is subvertical. This deformation clearly postdates

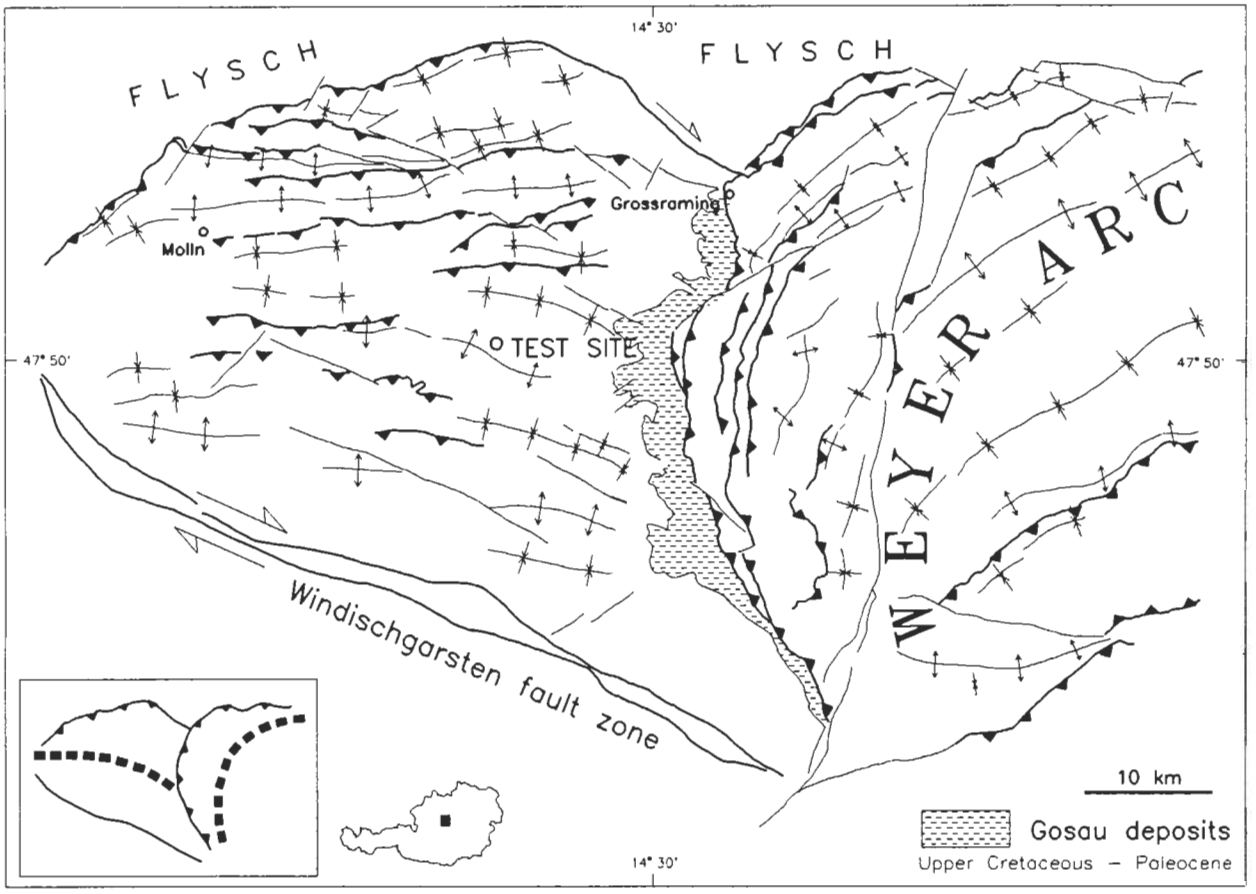

Fig. 4: Tectonic map of the Reichraming nappe and the Weyer Arc (simplified from DECKER et al., in prep.). Thick dashed line indicates strike directions of main folds and thrusts. The test site is located in the anticlockwise dragged part of Reichraming nappe. Dragging is caused by clockwise rotation and westward thrusting of the Weyer Arc.

the 45° rotation of set 1 and 2. Faults of favourable orientation belonging to these older sets and tilted bedding planes have been reactivated.

(4) Set 4 contains faults which cut all previously mentioned structures. They form a conjugate set of WSW–ENE striking sinistral and WNW–ESE striking dextral strike-slip faults. The dip angle of the fault planes is near 90°, striations are oriented subhorizontal. Shortening direction was E-W and extension N–S.

(5) Set 5 is the youngest feature at the test site consisting of pseudo-conjugate normal faults which dip steeply to the north or south. The northward dipping faults have been newly formed with pitch angles of about 90°, whereas most of the south dipping ones are reactivated older planes of sets 1, 2 and 3. Determination of the kinematic axes points out a N–S oriented extension.

Discussion of the results

Table 3 gives a comparison of different methods of fault-slip analyses applied to the 5 subsets. Column 2 shows the results of the P-T axes method (program FAULT) described above, column 3 gives the peak positions of the density grid counting of the P-, B- and T-axes, column 4 lists the results of a paleostress inversion program (SPERNER 1991) based on ANGELIER & GOGUEL (1978). The results of set 1 are very similar. Deviations between the different methods are less then 5° due to the relatively large number of data (N = 21) and the occurrence of conjugate faults. Set 2 shows very similar shortening directions. Although deformation is clearly of thrust type the inverse method gives oblique σ_2 and σ_3, axes whereas the P-T-axes method establishes a subvertical extension direction. The value of R% of the P-, B- and T-axes of set 1 and 2 is relatively high and similar to all the others proving triaxial strain. Results of the inverse method and the P-T axes method are very consistent for set 3 which consists mostly of reactivated faults. The value of R% of the P-axes at

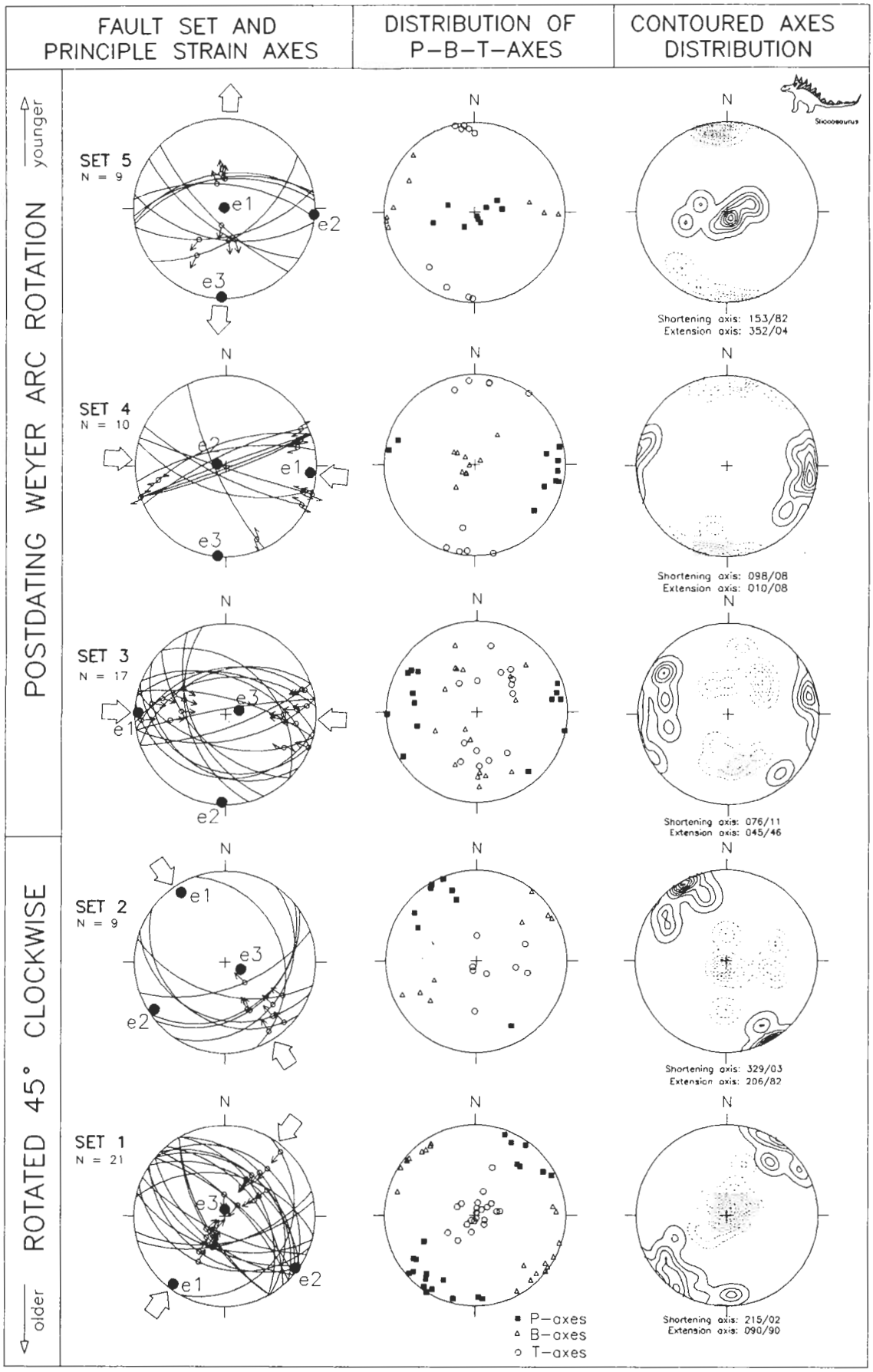
FAULT SET AND PRINCIPLE STRAIN AXES
DISTRIBUTION OF P–B–T–AXES
CONTOURED AXES DISTRIBUTION
younger
POSTDATING WEYER ARC ROTATION
ROTATED 45° CLOCKWISE
older
SET 5
N = 9
e1
e2
e3
Shortening axis: 153/82
Extension axis: 352/04
SET 4
N = 10
Shortening axis: 098/08
Extension axis: 010/08
SET 3
N = 17
Shortening axis: 076/11
Extension axis: 045/46
SET 2
N = 9
Shortening axis: 329/03
Extension axis: 206/82
SET 1
N = 21
Shortening axis: 215/02
Extension axis: 090/90
P–axes
B–axes
T–axes

Table 3: Comparison of the results of fault slip analysis for all subsets derived with different methods. Column 2 gives principle strain axes ($e_1 > e_2 > e_3$) of each subset computed with the P-T-axes method. Column 3 shows peak positions of contoured P-, B- and T-axes distribution. Column 4 lists paleostress directions ($\sigma_1 > \sigma_2 > \sigma_3$) obtained with the inverse methode (SPERNER 1991) using an algorithmus proposed by ANGELIER & GOGUEL (1978). The results of all methods are well comparable. See text for discussion.

1	2		3	4
Fault set	**Center of gravity vectors of P-, B-, T-axes (Θ = 45°)**		**Peak position of density grid counting**	**Inverse method**
Set 1	e_1: 217/07	R % = 83 %	e_1: 215/02	σ_1: 220/05
N = 21	e_2: 126/03	R % = 88 %	e_2: 126/02	σ_2: 130/00
	e_3: 004/84	R % = 90 %	e_3: 090/90	σ_3: 040/85
Set 2	e_1: 328/10	R % = 89 %	e_1: 329/03	σ_1: 341/05
N = 9	e_2: 236/08	R % = 81 %	e_2: 061/06	σ_2: 246/48
	e_3: 113/74	R % = 78 %	e_3: 206/82	σ_3: 075/42
Set 3	e_1: 272/06	R % = 77 %	e_1: 076/11	σ_1: 275/05
N = 17	e_2: 182/04	R % = 24 %	e_2: 176/30	σ_2: 185/05
	e_3: 074/77	R % = 50 %	e_3: 045/46	σ_3: 050/83
Set 4	e_1: 098/09	R % = 92 %	e_1: 098/08	σ_1: 075/10
N = 10	e_2: 284/83	R % = 92 %	e_2: 236/78	σ_2: 330/56
	e_3: 187/01	R % = 90 %	e_3: 010/07	σ_3: 172/32
Set 5	e_1: 124/89	R % = 80 %	e_1: 153/83	σ_1: 181/77
N = 9	e_2: 095/03	R % = 83 %	e_2: 263/01	σ_2: 272/00
	e_3: 183/02	R % = 84 %	e_3: 353/04	σ_3: 003/13

Fig. 5: (left side:) Plot of all 5 subsets derived from 66 faults at the test site. All diagrams are equal area lower hemisphere plots. Left column: Plot of fault planes (great circles) and striations (small arrows indicating movement of hanging wall); e_1, e_2 and e_3 denote the three principle strain axes computed with the P-T axes method (e_1 = mean shortening direction, e_3 = mean extension direction). Large arrows indicate azimuth of shortening (set 1–4) or extension directions (set 5). Mid column: Plot of computed P-axes (filled squares), B-axes (triangles) and T-axes (circles) of each individual fault of one subset. Right column: Contoured distribution of P-axes (solid lines) and T-axes (dashed lines). Peak positions are given below each diagram.

set 3 is considerably higher than that of the B- and T-axes, which points to uniaxial shortening and to an oblate shape of the strain ellipse. In this case, peak positions of the density grid counting method leads to no satisfying results because of the large diversity of the P-, B- and T-axes and therefore of the lack of clearly defined peak positions. Set 4 comprises conjugate strike-slip faults formed by E–W shortening. This data set shows best the advantage of the P-T axes method in case of conjugate faults. The shortening axis is oriented 098/09 (E–W), the extension axis trends N–S (187/01). The inverse method fails in this case giving a σ_1 direction of 075/10 which is almost parallel to the dextral faults of set 4.

The results determined by the three methods for set 5 again are very similar. The R% values are high for all three axes and point to triaxial strain. The south dipping faults in set 5 are reactivated planes with larger directional diversity than the north dipping ones. Therefore, the inverse method gives well

constrained results although the number of faults is low (N = 9). The determined directions of the principle stress axes coincide well with the strain axes derived from the P-T-axes method.

The derived chronology of deformation types and shortening directions fits well into the general succession in other parts of the Northern Calcareous Alps as figured out by DECKER et al. (1992).

6. Conclusions

The described determination of the principle incremental strain axes for a given fault set using the P- and T-axes together with careful interpretation of field criteria provides reliable information about brittle deformations. Obtained results are very robust and not affected by single non-fitting faults. This method gives the best results in case of newly formed conjugate faults with a relatively similar development of both sets (set 4). Subset 3 of the test site shows the usefulness of this method even in case of reactivated fault sets. Only few data are necessary to get a good estimation of shortening and extension directions whereas most other methods need a quite larger amount of data. The graphical presentation of the data set and the results help to avoid artifical or geologically meaningless interpretations. A manual preseparation of kinematically compatible faults into cogenetic subsets is necessary. This procedure is supported by suggestions of the software which uses main movement characteristics on fault planes as criteria for automatic preseparation. However, a combined kinematic and dynamic analysis with different methods is the best way to get objective informations.

Acknowledgements

I thank K. Decker for his critical review of this paper and for many suggestions and ideas and M. Jarnik and I. Peresson for viewing the manuscript.

7. References

ALEXANDROWSKI, P. (1985): Graphical determination of principal stress directions for slickenside lineation population: an attempt to modify Arthaud's method. — J. Struct. Geol., **7,** 73–82, Oxford.

ANDERSON, E. M. (1951): The dynamics of faulting. — 83 S., London (Oliver & Boyd).

ANGELIER, J. & MECHLER, P. (1977): Sur une méthode graphique de recherche des contraintes principales également utilisable en tectonique et en séismologie: la méthode des dihdres droits. — Bull. Soc. Géol. Fr., 7 Sér., **19,** 1309–1318, Paris.

— (1979): Determination of the mean principal directions of stress for a given fault population. — Tectonophysics, **56,** T17–T26, Amsterdam.

— (1984): Tectonic analysis of fault-slip data sets. — J. Geophys. Res., **89,** 5835–5848, Washington.

ARMIJO, R., CAREY, E. & CISTERNAS, A. (1982): The inverse problem in microtectonics and the separation of tectonic phases. — Tectonophysics, **82,** 145–160, Amsterdam.

ARTHAUD, F. (1969): Méthode de detérmination graphique des directions de raccourcissement, d'allongement et intermediaire d'une population de failles. — Bull. Soc. Géol. Fr., **11,** 729–737, Paris.

BOTT, M. H. P. (1959): The mechanics of oblique slip faulting. — Geol. Mag., **96,** 109–117, Cambridge.

CAPUTO, M. & CAPUTO, R. (1988): Structural analysis: new analytical approach and application. — Annales Tectonicae, **2,** 84–89, Florenz.

CASAS-SAINZ, A. M. & SIMÓN-GÓMEZ, J. L. (1992): Stress field and thrust kinematics: a model for the tectonic inversion of the Cameros Massif (Spain). — J. Struct. Geol., **14,** 521–530, Oxford.

DECKER, K., RING, U. & MESCHEDE, M. (1992): Paleostresses derived from fault-slip analysis in the northern part of the Eastern Alps: Molasse, Helvetic nappes, Rhenodanubic Flysch and Calcareous Alps. — Terra abstracts: ALCAPA – Geological evolution of the internal Eastern Alps, Carpathians and of the Pannonian basin, Graz (Austria). — Abstract supplement No. 2 to Terra nova, **4**/(1992), 15–16, Oxford.

ETCHECOPAR, A., VASSEUR, G. & DAIGNIERES, M. (1981): An inverse problem in microtectonics for the determination of stress tensors from fault striation analysis. — J. Struct. Geol., **3,** 51–65, Oxford.

FRITZ, H., SCHRADER, F. & WALLBRECHER, E. (1990): Analysis of kinematics in faulted rocks: A methodical comparison with an example from the Eastern Alps (Austria). — Jb. Geol. B.-A., **133,** 549–560, Wien.

GALINDO-ZALDIVAR, J. & GONZALES-LODEIRO, F.(1988): Faulting phase differentiation by means of computer search on a grid pattern. — Annales Tectonicae, **2,** 90–97, Florenz.

GEPHART, J. W. (1990): Stress and the direction of slip on fault planes. — Tectonics, **9,** 845–858, Washington.

HANCOCK, P. L. (1985): Brittle microtectonics: principles and practice. — J. Struct. Geol., **7,** 437–457, Oxford.

HOEPPENER, R. (1955): Tektonik im Schiefergebirge. — Geol. Rundschau, **44,** 26–58, Stuttgart.

HUANG, Q. & ANGELIER, J. (1989): Inversion of field data in fault tectonics to obtain the regional stress-II. Using conjugate fault sets within heterogeneous families for computing palaeostress axes. — Geophys. J., **96,** 139–149.

LISLE, R. J. (1987): Principal stress orientation from faults: an additional constraint. — Annales Tectonicae, **1,** Nr. 2, 155–158, Florenz.

MANDL, G. (1988): Mechanics of tectonic faulting: Models and basic concepts. — 407 S., Amsterdam (Elsevier).

MARRETT, R. & ALLMENDINGER, R. W. (1990): Kinematic analysis of fault-slip data. — J. Struct. Geol., **12,** 973–986, Oxford.

MEANS, W. D. (1987): A newly recognized type of slickenside striation. — J. Struct. Geol., **9,** 585–590, Oxford.

MICHAEL, A. J. (1984): Determination of stress from slip data: Faults and folds. — J. Geophys. Res., **89,** 517–526, Washington.

ONCKEN, O. (1988): Aspects of the reconstruction of the stress history of a fold and thrust belt (Rhenish massif, Federal Republic of Germany). — Tectonophysics, **152,** 19–40, Amsterdam.

PERESSON, H.(1991): Kinematische Analyse von Störungsflächen und Folgerungen für die strike-slip Tektonik an der Wolfgangseestörung (Salzburg). — Dipl.-Arb. Univ. Wien, 116pp., Wien.

— (1992): Kinematische Analyse der Wolfgangseestörung (Kalkalpen, Oberösterreich). — Frankfurter geowiss. Arb., Serie A, **11,** 277–279, Frankfurt a. M.

PETIT, J. P., PROUST, F. & TAPPONNIER, P. (1983): Critères de sens de mouvement sur les miroirs de failles en roches non calcaires. — Bull. Soc. géol. Fr., **25,** 589–608, Paris.

— (1987): Criteria for the sense-of-movement on fault surfaces in brittle rocks. — J. Struct. Geol., **9,** 597–608, Oxford.

PFIFFNER, O. A. & BURKHARD, M. (1987): Determination of paleostress axes orientation from fault, twin and earthquake data. — Annales Tectonicae, **1,** 48–57, Florenz.

RAMSAY, J. G. & HUBER, M. I., (Eds.) (1983): The techniques of modern structural Geology: Volume **I,** strain analysis. — 307pp., London (Acad. Press).

— & — (1987): The techniques of modern structural Geology: Volume II, folds and fractures. — 700pp., Orlando, Florida (Academic Press).

RECHES, Z. (1987): Determination of the tectonic stress tensor from slip along faults that obey the Coulomb yield condition. — Tectonics, **6,** 849–861, Washington.

ROBIN, P.-Y. F. & JOWETT, C. (1986): Computerized density contouring and statistical evaluation of orientation data using counting circles and continuous weighting functions . — Tectonophysics, **121,** 207–223, Amsterdam.

SPERNER, B. (1991): Analyse der Deckenkinematik mit Hilfe von Spröddaten an einem Beispiel aus den Nördlichen Kalkalpen (niederösterreichische Kalkvoralpen). — Dipl.-Arb. Univ. Tübingen, 127pp., Tübingen.

TOLLMANN, A. (1962: Die Rolle des Ost-West Schubes im Ostalpenbau. — Mitt. Geol. Ges. Wien, **54**/(1961), 229–247, Wien.

— (1969): Tektonische Karte der Nördlichen Kalkalpen. — 2. Teil: Der Mittelabschnitt. — Mitt. Geol. Ges. Wien, **61**/(1968), 124–181, Wien.

WALLACE, R. E. (1951): Geometry of shearing stress and relation to faulting. — J. Geol., **59,** 118–130.

WALLBRECHER, E. (1986): Tektonische und gefügeanalytische Arbeitsweisen. — 244pp., Stuttgart (Encke).

— & FRITZ, H. (1989): Quantitative evaluation of the shape factor and the orientation of a paleostress ellipsoid from the distribution of slickenside striations. — Annales Tectonicae, **3,** 110–122, Florenz.

WOJTAL, S. & PERSHING, J. (1991): Paleostresses associated with faults of large offset. — J. Struct. Geol., **13,** 49–62, Oxford.